

Online energy management system for a fuel cell/battery hybrid system with multiple fuel cell stacks

Junzhe Shi¹, Ulf Jakob Flø Aarsnes², Dagfinn Nærheim³, Scott Moura^{4*}

1. University of California, Berkeley, Department of Civil and Environmental Engineering, 760 Davis Hall, Berkeley, CA 94720, USA. Berkeley, CA 94720, USA. junzhe@berkeley.edu
2. NORCE, Postboks 22, Nygårdstangen 5838 Bergen. ulaa@norceresearch.no
3. Corvus Energy, Sandbrekktoppen 30, 5224 Nesttun, Bergen, Norway. dnaerheim@corvusenergy.com
4. University of California, Berkeley, Department of Civil and Environmental Engineering, 760 Davis Hall, Berkeley, CA 94720, USA. Berkeley, CA 94720, USA. smoura@berkeley.edu

* Corresponding author: Scott Moura, University of California, Berkeley, Department of Civil and Environmental Engineering, 760 Davis Hall, Berkeley, CA 94720, USA, Email: smoura@berkeley.edu

Abstract— In recent years, fuel cell/battery hybrid systems have attracted substantial attention due to their high energy density and low emissions. The online energy management system (EMS) is essential for these hybrid systems, tasked with controlling the energy flow and ensuring optimal system performance, encompassing fuel efficiency and mitigating fuel cell and battery degradation. This research proposes a novel approach to energy management for hybrid fuel cell/battery systems with multiple fuel cell stacks. It introduces an online EMS that employs Mixed Integer Quadratic Programming (MIQP) to independently control each fuel cell stack in the hybrid system. The performance of this method is compared to Dynamic Programming (DP), a standard approach for energy management in such systems. Results demonstrate that the proposed method achieves superior computational efficiency compared to DP while delivering improved performance. Furthermore, the research reveals that independent control of multiple stacks results in a more optimized system operation compared to traditional methods, which consider multiple stacks as a single entity and implement identical control actions across all.

Keywords—*Energy management system, fuel cell, battery, MIQP, hybrid system*

I. INTRODUCTION

A. Background and Motivation

The escalating demand for clean, efficient, and reliable energy systems has stimulated the evolution of fuel cell (FC) and battery hybrid systems. These systems offer an array of advantages including high efficiency, load leveling, extended operating range, reduced emissions, and heightened reliability [1]. The amalgamation of fuel cells and batteries forms a robust and environmentally friendly power source, accommodating various applications from transportation to stationary power generation [2].

However, a significant barrier to the broad adoption of hydrogen as an energy source lies in the high aggregate cost of fuel cell systems and hydrogen fuel [3]. This issue is further compounded by fuel cell degradation during particular operating conditions, leading to reduced lifetime and elevated operating expenses [4].

Certain applications, such as city buses, trucks, and ocean-going vessels, necessitate long operating times and high transient loads, making the incorporation of multiple fuel cell stacks in the hybrid systems essential. Using multiple fuel cells enhances the system capability by offering scalability, load sharing, redundancy, and a modular design. The use of multiple FC stacks, each controlled individually, presents opportunities to augment overall system efficiency, reliability, and lifespan [5]. Nevertheless, attaining optimal performance from such systems requires consideration of both the cost of fuel and system degradation in the energy management strategy (EMS), which oversees the power distribution among FCs and batteries.

The design of an effective EMS that can grapple with the complexities presented by multiple fuel cell stacks, while acknowledging the dynamic nature of the system, is a significant challenge. This research paper is motivated by the intent to address this challenge by devising an optimal and efficient EMS for fuel cell and battery hybrid systems with multiple FC stacks. This approach takes into consideration fuel consumption cost, battery degradation, and FC degradation.

B. Literature review

Numerous strategies have been proposed for EMS design, typically falling into three categories: optimization-based control, rule-based control, and learning-based control.

Optimization-based control formulates the EMS design as an optimization problem, aiming to find optimal control actions that minimize a specific objective function. Dynamic

Programming (DP) and Pontryagin's Minimal Principle (PMP) are the most common methods utilized to solve optimization problems. In [6], a DP-based EMS aims to primarily reduce fuel consumption and battery degradation. An EMS based on PMP focuses on hydrogen consumption reduction [7], while [8] employs an adaptive recursive least square method with PMP to maximize PEMFC power efficiency. The strength of optimization-based control lies in its ability to locate globally optimal solutions, considering various constraints and system dynamics. However, this method often demands significant computational resources and may be ill-suited for real-time applications in complex systems.

Rule-based control, popular for real-time control applications, employs predefined rules and thresholds for power distribution between the FC and battery. Rules typically hinge on the state of charge (SOC) of the battery, the power demand of the load, and other operational parameters. To improve computational efficiency for online operation while maintaining optimality, rules are usually derived from optimization results. A rule-based EMS for FC hybrid trains, developed based on DP results under various driving conditions, is presented in [9]. Besides, [10] generates an optimized rule-based EMS using the genetic algorithm to optimally allocate the power between the fuel cell and the battery system. Rule-based control is relatively simple to implement and computationally efficient. However, it may not provide optimal performance since it does not account for all the system dynamics or adapt to changing conditions.

Learning-based control methods, like Neural Networks (NN) and Reinforcement Learning (RL), are also employed to enhance the computational time of optimization-based control methods. These methods may continually adapt and improve control actions through system interactions and feedback. NN can handle complex and non-linear system dynamics, but often requires substantial training data. In [11], eight NNs, trained by selected optimization results, aim to minimize the overall equivalent energy consumption while reducing the high computational cost of optimization. RL is a type of machine learning method, and it utilizes an agent to make decisions through interaction with its environment and feedback in the form of rewards or penalties. A Q-learning-based EMS to minimize battery degradation and energy consumption for hybrid vehicles is proposed in [12]. Similarly, a deep Q-learning-based EMS, designed to improve fuel economy and extend fuel cell lifetime for FC hybrid electric vehicles, is proposed in [13]. However, RL may only find a locally optimal or suboptimal solution, unlike DP, which guarantees the finding of a global optimal solution. Also, RL methods can be time-consuming and computationally expensive during training as they may require numerous episodes to converge.

Despite the promise, few works focus on EMS design with multiple FC stacks. While [14] presents three power splitting algorithms for multiple FC stacks to optimize the efficiency of a multi fuel cell system, the method cannot be directly applied to hybrid systems and neglects FC system degradation. [15]

uses an adaptive state machine strategy to increase the lifetime of the FCS, though it overlooks many factors contributing to system degradation, leading to potentially suboptimal results. [16] employs independent Q-learning to maintain battery SOC and minimize hydrogen consumption for a multi-stack fuel cell system, but this work inherits the drawbacks of RL methods.

Despite the rising interest in hybrid electric vehicles and EMS design, several research gaps remain. A novel, efficient, and optimal EMS design method that overcomes the limitations of existing optimization-based control, rule-based control, and learning-based control methods is needed. While several studies have investigated the performance of individual fuel cell stacks, research focusing on the optimal operation and control of multiple fuel cell stacks within a hybrid system is lacking, particularly in terms of minimizing the costs related to system efficiency, and degradations of batteries and FCs.

C. Contribution

To fill the above research gaps, this paper extends the existing research by developing a novel EMS for a hybrid energy system, inspired by the limitations of DP in managing the complexity of multiple FC stacks.

The key contributions and novelties of this study include:

1. This research addresses the need for efficient and optimal EMS design by considering the optimization of multiple FC stacks in a hybrid energy system. The control strategy differs significantly from controlling a single FC stack.
2. The paper proposes a novel reformulation of optimal control for the fuel cell hybrid system that suits Mixed-Integer Quadratic Programming (MIQP). This reformulation enables the efficient and effective resolution of the optimization problem, offering a practical solution for real-time implementation that overcomes the complexity challenges of DP.
3. The research highlights the advantages of independent stack control in the hybrid system. By controlling multiple fuel cell stacks independently rather than as a collective stack with identical control actions, superior performance is achieved.

D. Organization of the Paper

The organization of this paper is as follows. Section II introduces the models of the vehicle, battery, and fuel cell employed in this study. The methodologies for the reformulation of optimal control for the fuel cell hybrid system that aligns with MIQP are discussed in Section III. Section IV provides an analysis of the simulation results of the proposed system. Lastly, Section V encapsulates the key conclusions drawn from this study.

II. MODEL

In order to demonstrate the effectiveness of the proposed method, this study employs an electric hybrid city bus as the representative model for the FC and battery hybrid system. The first subsection delves into the operational dynamics and system structures of a city bus powered by hybrid electric energy. Following that, the next two subsections respectively discuss the specific battery and fuel cell models employed in this research.

A. Vehicle Model and System Configurations

The goal of the hybrid electric vehicle model is to transform a driving cycle's velocity profile into a corresponding power demand profile. The formulation of the vehicle dynamic model can be expressed as [17],

$$P_V = m g f v \cos(\alpha) + 0.5 C_D A_f \rho v^3 + m v \frac{dv}{dt} + m g v \sin(\alpha) \quad (1)$$

$$P_d = \begin{cases} P_V \eta_T \eta_{md} & \text{if } P_V > 0 \\ \frac{P_V}{\eta_r} & \text{if } P_V \leq 0 \end{cases} \quad (2)$$

Here, P_V denotes the power required to counteract road friction, air drag, and gravitational pull. The power demand (P_d), for a city bus is determined by considering the transmission efficiency (η_T), electrical machine efficiency (η_{md}), and the efficiency of regenerative braking (η_r). The remaining parameters are defined and described in TABLE I [18].

TABLE I

Parameters and Description of the Electric City Bus		
Parameter	Description	Value
m	Vehicle mass	13500 kg
E_{\max}	Maximum energy capacity	293 kWh
g	Gravity acceleration	9.8 m/s ²
A_f	Front area	7.5 m ²
f	Rolling resistance coefficient	0.018
C_D	Air drag coefficient	0.7
ρ	Air density	1.29 kg/m ³
η_T	Transmission efficiency	90%
η_{md}	Electrical machine efficiency	85%
η_r	Regenerative braking efficiency	50%

Fig. 1 illustrates the structure of the semi-active hybrid energy storage system. The electric motor propels the rear wheels. Positioned between the electric motor and the two energy storage systems is a DC/AC converter. To balance the voltage between the battery pack and fuel cell stacks, the AC/DC converter and DC/DC converters are utilized. In the hybrid system, there are one battery pack and multiple fuel cell stacks.

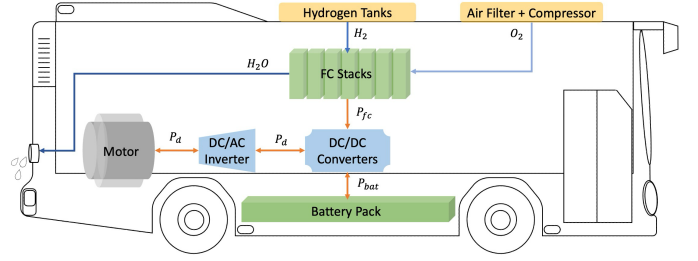


Fig. 1. Architecture of the FC hybrid bus propulsion system.

B. Battery Model

1) Battery Electrical Model

In this research, an equivalent circuit model (ECM), also known as the Rint model, is utilized to simulate the electrical characteristics of a battery. The ECM comprises an open-circuit voltage (OCV) and an ohmic resistor (R_0). The terminal voltage (V_T) is the output of the ECM. The values for the OCV and R_0 are dependent on the SOC (in %), temperature, and both discharge and charge currents [19].

The dynamic of a battery can be formulated as follows,

$$SOC(i) = SOC(i-1) + \frac{100\% \Delta t I}{3600 Q_{bat}} \quad (3)$$

$$V_T = OCV + R_0 I \quad (4)$$

where I (in A) is the current, Δt (in s) is sampling time, and Q_{bat} (in Ah) is the nominal capacity.

2) Battery Degradation Model

The study employs an empirical degradation model for the Li-ion battery, as sourced from [20]. This model describes the loss in battery capacity (Q_{loss} , in %) as a function of several variables, including temperature (T , in K), C-rate (c_{rate}), and Ampere-hour throughput (Ah).

$$Q_{loss} = M(c_{rate}) \exp\left(\frac{-E_a}{RT}\right) (Ah)^z \quad (5)$$

$$Ea = a_c + b_c C_{rate} \quad (6)$$

where R signifies the ideal gas constant, while E_a is the activation energy. The power law factor is represented by z and set to 0.55. The two fitting parameters a_c and b_c are 31700 and 370.3. The parameter, M , is a pre-exponent factor that diminishes as the C-rate increases, as demonstrated in TABLE II [21].

TABLE II PRE-EXPONENTIAL FACTOR AS A FUNCTION OF THE C-RATE				
C-rate	0.5	2	6	10
M	31630	21681	12934	15512

C. Fuel Cell Model

Proton Exchange Membrane (PEM) fuel cells are favored in electric vehicles and hybrid energy systems due to their high energy efficiency, fast startup and response times, low operating temperature, compact design, environmental friendliness, quiet operation, and scalability [22]. They offer a promising solution for clean and efficient power generation. As such, all the FCs utilized in this study are assumed to be of the PEM type.

1) Fuel Cell Power to mass flow rate curve

Fig. 2 presents the consumption and efficiency curve of a FC system, derived from the Advanced Vehicle Simulator (ADVISOR, a scaled version of FC_ANL50H2). The correlation between mass flow rate and the power of a fuel cell per unit effective catalyst surface area is illustrated in Fig. 3. Owing to the demonstrated precision of a quadratic function in replicating fuel cell hydrogen consumption [23], a quadratic function has been employed to approximate the map illustrating hydrogen consumption in relation to the power output of the fuel cell, as depicted below,

$$\dot{m} = a_m P_{fc}^2 + b_m P_{fc} + c_m \quad (7)$$

In this equation, \dot{m} signifies the mass flow rate, P_{fc} stands for the output power of a fuel cell per unit effective catalyst surface area, while a_m , b_m , and c_m are fitting parameters.

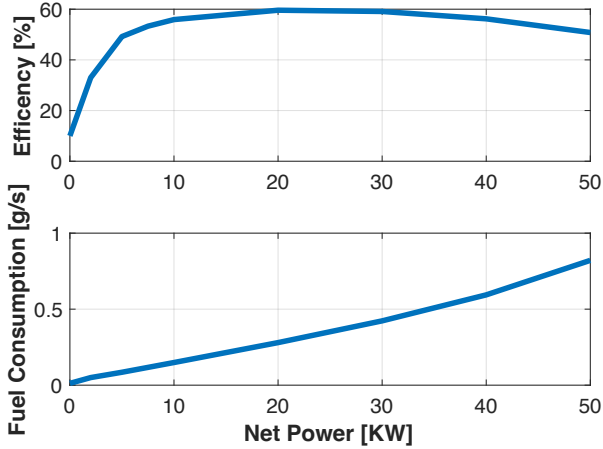


Fig. 2. Fuel cell efficiency and fuel consumption curves.

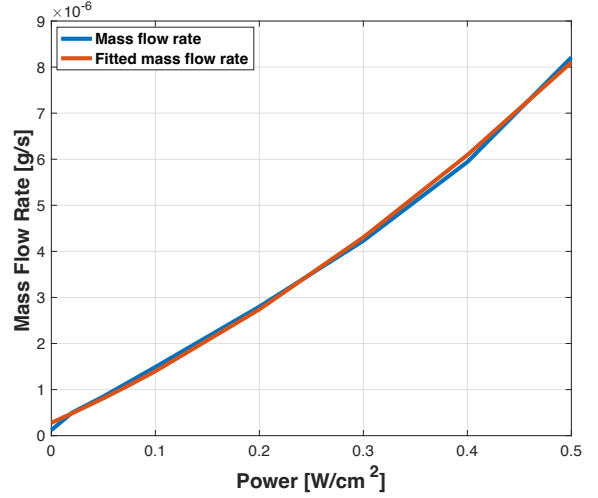


Fig. 3. Fuel cell power per unit effective catalyst surface area vs. mass flow rate.

2) Fuel Cell Degradation Model

The voltage of a fuel cell is determined by the polarization equation [24] as shown below:

$$V = V_{ocv} - V_{act} - V_{ohm} - V_{con} \quad (8)$$

In this context, V_{ocv} is the reversible cell voltage, which would be achieved if Gibbs free energy could convert directly into electrical work without any losses. V_{act} refers to activation polarization, which arises due to slow oxidation and/or reduction kinetics at the electrode surface. V_{ohm} is indicative of ohmic voltage losses, which are caused by resistance to electron flow through the fuel cell components. V_{con} signifies the voltage drop that occurs due to challenges in supplying sufficient reactants to the catalyst sites as the demand for current rises. The respective equations for these terms are,

$$E_{ocv} = -\frac{\Delta G}{2F} \quad (9)$$

$$V_{act} = \alpha T \ln\left(\frac{I_{fc} + i_{loss}}{i_0}\right) \quad (10)$$

$$V_{ohm} = R_o I_{fc} \quad (11)$$

$$V_{con} = -\beta \ln\left(1 - \frac{I_{fc}}{i_l}\right) \quad (12)$$

Here, ΔG represents Gibbs free energy, F stands for Faraday's constant, and T is the temperature, while I_{fc} signifies the current density. Furthermore, R_o refers to cell internal resistance, α denotes the charge transfer coefficients, i_{loss} is the crossover current density, i_0 indicates the exchange current density, β is an empirically fitted constant, and i_l is the maximum current density.

Certain operations, such as altering load, toggling the start-stop condition, idling, and handling high-power loads, significantly contribute to the degradation of the fuel cell [25]. The load change condition is tied to variations in the power supply of the fuel cell system over a sample period. The start-stop condition is activated by the on-off toggling of the fuel cell system. Idling and high-power conditions are initiated when the power supply of the fuel cell system falls within the respective low and high operational power ranges.

These operating conditions can lead to several detrimental outcomes, including corrosion, thermal stress/cycling, mechanical stress, drying/flooding, and impurities within the fuel cell systems [27] [28] [29] [30]. As depicted in Fig. 4, these

conditions subsequently cause the degradation of the fuel cells' components, such as the membrane, catalyst, gas diffusion layer, and bipolar elements [4] [31] [32] [33] [34] [35]. As shown in Fig. 4, these degraded components result in a decrease in charge transfer coefficient, an increase in internal current density and exchange current density, a rise in ohmic resistance, a decrease in maximum current density, and an increase in the concentration loss constant [3] [4] [27] [36]. These changes in R_o , α , β , i_{loss} , and i_0 , contribute to an increase in the voltage loss terms in the polarization equation, ultimately leading to power fade in the fuel cell system.

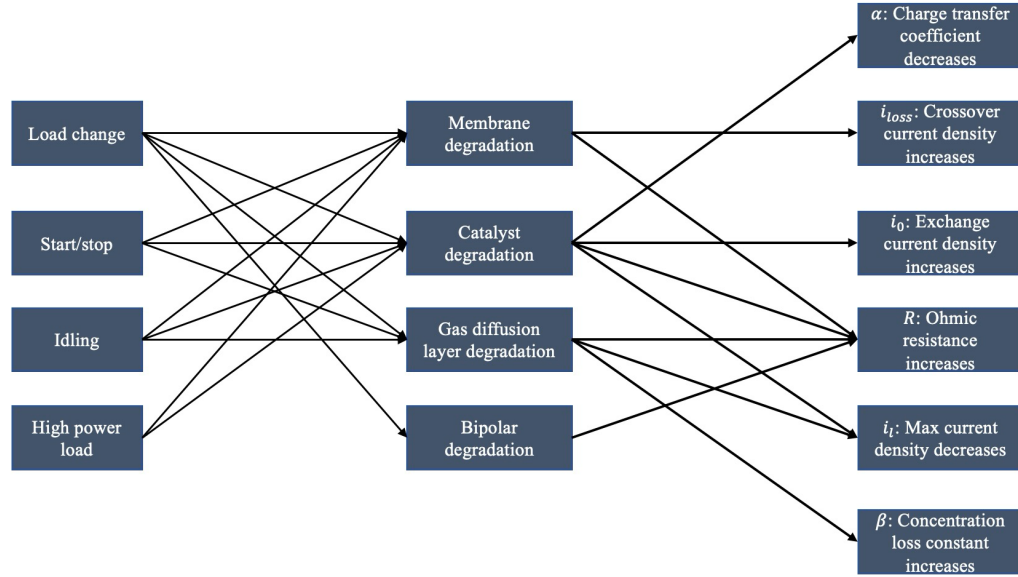


Fig. 4. Fuel cell degradations caused by four operational conditions.

Researchers in [25] and [31] conducted a series of experiments to distinguish the performance decline caused by transient operating conditions in a bus application and isolated their respective contributions to the performance deterioration of the fuel cell stack. TABLE III enumerates the voltage degradation rates of FC under different operating conditions. These voltage drop rates for the four conditions are referred to as $\Delta V_{load-change}$, ΔV_{on-off} , ΔV_{idling} , and $\Delta V_{high-load}$. If the cumulative voltage degradation surpasses 10% of the rated voltage of a new fuel cell, the fuel cell is regarded as reaching its end-of-life and needs replacement due to its diminished power efficiency [6].

TABLE III
VOLTAGE DEGRADATION RATES

Operations:	Symbols:	Drop rate:	
Load change	$\Delta V_{load-change}$	$1.79\mu\text{V}/\text{kW}$	
Start/Stop	ΔV_{on-off}	$13.79\mu\text{V}$	[37]
Idling	ΔV_{idling}	$8.66\mu\text{V}/\text{h}$	
High power load	$\Delta V_{high-load}$	$10\mu\text{V}/\text{h}$	[31]

The financial losses associated with the degradation of the FC system under four different operating conditions, $L_{load-change}$, L_{on-off} , L_{idling} , and $L_{high-load}$, can be calculated using the prescribed voltage degradation rates. The formulas for these calculations are as follows,

Load change:

$$L_{load-change} = \frac{|\Delta P| \Delta V_{load-change} C_{fc}}{V_{drop}^{max}} \quad (13)$$

On/off:

$$L_{on-off} = \begin{cases} \frac{\Delta V_{on-off} C_{fc}}{V_{drop}^{max}} & \text{if on/off triggered} \\ 0 & \text{otherwise} \end{cases} \quad (14)$$

Idling:

$$L_{idling} = \begin{cases} \frac{\Delta t \Delta V_{idling} C_{fc}}{3600 V_{drop}^{max}} & \text{if } 0 < P_{fc} \leq P_{fc}^{low} \\ 0 & \text{if } P_{fc} > P_{fc}^{low} \end{cases} \quad (15)$$

High power load:

$$L_{high-load} = \begin{cases} \frac{\Delta t \Delta V_{high-load} C_{fc}}{3600 V_{drop}^{max}} & \text{if } P_{fc} \geq P_{fc}^{high} \\ 0 & \text{if } P_{fc} < P_{fc}^{high} \end{cases} \quad (16)$$

In these formulas, ΔP (in kW) denotes the power change of the FC system over a sampling time, C_{fc} (in \$/kW) represents the total cost of the FC stacks, V_{drop}^{max} (in μV) indicates the maximum allowed cumulative voltage drop of the FC due to degradation, and Δt (in second) represents the sampling time of the system. The thresholds for low and high power denoted as P_{fc}^{low} and P_{fc}^{high} , are designated as 0.2 and 0.8 of the maximum power supply capability of the fuel cell system, respectively [26].

III. METHODOLOGY

In this section, the initial subsection focuses on the cost function of the hybrid system. The cost function is a crucial element in the optimization problem and warrants detailed examination. Following this, the subsequent part of the section explores the reformulation of constraints within the cost function. The objective is to facilitate the resolution of the optimization problem using the MIQP method. By restructuring the constraints, the aim is to simplify the problem representation and enable efficient computation of the optimal solution. In the final subsection, the selection of the solver for the MIQP is discussed.

A. Cost Function of the Hybrid System

To minimize the operational cost over a specified time horizon and power demand profile, determining the optimal sequential actions for each FC stack and the battery pack in the hybrid system becomes imperative. This goal involves minimizing the degradation losses of both the fuel cell stacks and the battery pack, along with the fuel consumption cost of the fuel cells. Thus, we can formulate the goal as an optimization problem, represented by the following equation,

$$J = \sum_{i=1}^N \sum_{j=1}^M \dot{m}(i, j) \Delta t C_{H_2} + l_{fc}(i, j) + l_{bat}(i) \quad (17)$$

In this equation, i denotes the current time step within the total time horizon N , while j corresponds to a specific fuel cell stack, with M being the total number of FC stacks in the system. The fuel consumption cost is calculated based on the mass fuel rate $\dot{m}(i, j)$ (in kg/s) of a given FC stack j at time i , the sampling time Δt (in s), and the hydrogen price C_{H_2} (in \$/kg). The loss term, $l_{fc}(i, j)$ represents the total degradation losses (in \$)

incurred by FC stacks j at time step i , respectively. The loss term, $l_{bat}(i)$ refers to Eq. (5) and represents the total degradation losses (in \$) for the battery pack.

The cost function is subject to several constraints, including power constraints, FC dynamic constraints, and battery dynamic constraints. For all time step i , the constraints are described below,

Power constraint:

$$P_d(i) = P_{bat}(i) + \sum_{j=1}^M P_{fc}(i, j) \quad (18)$$

$$P_{fc}^{min} \leq P_{fc}(i, j) \leq P_{fc}^{max} \quad (19)$$

Fuel cell fuel consumption and degradation constraints:

$$\dot{m}(i, j) = f_{fc-fuel}(P_{fc}(i, j)) \quad (20)$$

$$l_{fc}(i, j) = l_{on-off}(i, j) + l_{load-change}(i, j) + l_{high-load}(i, j) + l_{idling}(i, j) \quad (21)$$

Battery dynamic and degradation constraints:

$$I_{bat}(i) = f_{bat-I}(P_{bat}(i), SOC_{bat}(i)) \quad (22)$$

$$I_{bat}^{min} \leq I_{bat}(i) \leq I_{bat}^{max} \quad (23)$$

$$SOC_{bat}(i+1) = SOC_{bat}(i) + \frac{100\% \Delta t I_{bat}(i)}{3600 Q_{bat}} \quad (24)$$

$$SOC_{bat}^{min} \leq SOC_{bat}(i) \leq SOC_{bat}^{max} \quad (25)$$

$$l_{bat}(i) = f_{bat-loss}(I_{bat}(i)) \quad (26)$$

The fuel cell dynamic constraints capture the fuel consumption, fuel cell degradation, and the power limitation of the fuel cell stacks. The power limitation of the fuel cell system is defined by P_{fc}^{min} and P_{fc}^{max} , representing the minimum and maximum power output of the fuel cell system. The function $f_{fc-fuel}(P_{fc}(i, j))$ refers to Eq. (7) and is used to calculate the hydrogen consumption rate, \dot{m} , based on the FC power and the FC power to mass flow rate curve, as shown in Fig. 3. The FC degradation terms, $l_{on-off}(i, j)$, $l_{load-change}(i, j)$, $l_{high-load}(i, j)$, and $l_{idling}(i, j)$ refer to Eq. (13-16) and represent degradation of the FC system under four different operating conditions. The battery dynamic constraints ensure that the battery operates within the desired SOC and current range. The function $f_{bat-I}(P_{bat}(i), SOC_{bat}(i))$ calculates the current, $I_{bat}(i)$, based on the given battery power and SOC. $I_{min_{bat}}$ and $I_{max_{bat}}$ represent the minimum and maximum current of the battery pack, while SOC_{bat}^{min} and SOC_{bat}^{max} define

the minimum and maximum SOC of the battery pack. Because batteries can be charged and discharged while FCs can only provide the positive power, I_{bat}^{min} is less than zero and P_{fc}^{min} equals to zero. The function $f_{bat-loss}(I_{bat}(i))$ calculates the battery degradation loss based on the given battery current.

It is important to note that several terms in the objective function and constraints, including $f_{fc-fuel}(P_{fc}(i, j))$, $f_{bat-loss}(I_{bat}(i))$, $l_{on-off}(i, j)$, $l_{load-change}(i, j)$, $l_{high-load}(i, j)$, $l_{idling}(i, j)$, and $f_{bat-l}(P_{bat}(i), SOC_{bat}(i))$ are highly nonlinear. Consequently, the subsequent subsections will delve into the reformulation of these highly nonlinear terms to enable their inclusion in the MIQP optimization problem. The reformulation process aims to transform these nonlinear terms into linear or quadratic forms, thereby facilitating their incorporation into the optimization framework.

B. Fuel Cell Power to Mass Flow Rate

As mentioned in section II.C.1), the hydrogen consumption of the FC stack can be effectively approximated by a quadratic function based on the FC power. However, if we directly apply the power-to-mass flow function in the optimization, the mass flow rate remains non-zero even when the output power is zero. To accurately capture the on-off mechanism of the FC stack, an additional logic is introduced.

To achieve this, a binary control variable, $o_{fc}(i, j)$, is introduced to represent the “on” condition of the fuel cell stack j at time step i . The following constraints ensure that $o_{fc}(i, j)$ is set to zero when the power output of the FC stack, $P_{fc}(i, j)$, is lower than P_{fc}^{min} , and it is set to one otherwise,

$$o_{fc}(i, j) P_{fc}^{min} \leq P_{fc}(i, j) \quad (27)$$

$$P_{fc}(i, j) \leq o_{fc}(i, j) P_{fc}^{max} \quad (28)$$

By incorporating these constraints, $f_{fc-fuel}(P_{fc}(i, j))$ can be reformulated as a quadratic function and included in the objective function,

$$\begin{aligned} \dot{m}(i, j) = & a_{fc} P_{fc}(i, j)^2 + b_{fc} P_{fc}(i, j) \\ & + c_{fc} o_{fc}(i, j) \end{aligned} \quad (29)$$

where, a_{fc} , b_{fc} , and c_{fc} are fitted parameters that capture the characteristics of the power-to-mass flow relationship for the FC stack. This reformulation ensures that the mass flow rate is forced to zero when the FC stack is turned off, and allows for accurate representation of the FC stack's behavior, accounting for both power output and the on-off status of the stack.

C. FC loss due to on-off switch and load changes

In this subsection, the reformulations of the FC loss terms resulting from on-off switching and load changing are discussed.

As discussed in section II.C.2), calculating the FC loss terms requires determining whether an on-off switch has occurred and expressing the absolute value of the power change. To capture these aspects, we introduce two variables for each time step i and FC stack j : the binary variable $s_{fc}(i, j)$ and the positive variable $\Delta P_{fc}^+(i, j)$.

The binary control variable $s_{fc}(i, j)$ is set to one if there is a change from $o_{fc}(i-1, j)$ to $o_{fc}(i, j)$. Otherwise, it is forced to zero by the cost function. The following constraints represent this relationship,

$$s_{fc}(i, j) \geq o_{fc}(i, j) - o_{fc}(i-1, j) \quad (30)$$

$$s_{fc}(i, j) \geq o_{fc}(i-1, j) - o_{fc}(i, j) \quad (31)$$

The variable $\Delta P_{fc}^+(i, j)$ is constrained to represent the absolute value of the power change, $|P_{fc}(i, j) - P_{fc}(i-1, j)|$, using the following equations,

$$\Delta P_{fc}^+(i, j) \geq P_{fc}(i-1, j) - P_{fc}(i, j) \quad (32)$$

$$\Delta P_{fc}^+(i, j) \geq P_{fc}(i, j) - P_{fc}(i-1, j) \quad (33)$$

With these variables in place, we can rewrite the Eq. (13) and Eq. (14) and express the FC degradation loss terms $l_{load-change}(i, j)$ and $l_{on-off}(i, j)$ as follows,

$$l_{load-change}(i, j) = \frac{\Delta V_{load-change} C_{fc}}{V_{drop}^{max}} \Delta P_{fc}^+(i, j) \quad (34)$$

$$l_{on-off}(i, j) = \frac{\Delta V_{on-off} C_{fc}}{V_{drop}^{max}} s_{fc}(i, j) \quad (35)$$

where ΔV_{on-off} and $\Delta V_{load-change}$ represent the voltage degradation rates due to on-off switching and load changing, as shown in TABLE III. C_{fc} is the price of the fuel cell, and V_{drop}^{max} is the maximum allowed cumulative voltage drop due to degradation. These formulations ensure that the loss terms accurately capture the effects of on/off switching and load changing on the FC stack.

D. FC Degradation Loss Terms due to High Power Load and Idling Reformulation

In this subsection, the reformulation of the FC degradation loss terms due to high power load and idling conditions are discussed.

As discussed in section II.C.2), it is necessary to identify whether an FC stack is operating under high power load or idling conditions when calculating the FC degradation loss terms. We introduce two variables for each time step i and FC stack j to capture these aspects: the binary variables $h_{fc}(i, j)$ and $i_{fc}(i, j)$.

To enforce the binary variable $h_{fc}(i, j)$ to indicate whether the power of FC stack j is larger than P_{fc}^{high} at time step i , the following constraints are utilized,

$$\frac{P_{fc}(i, j) - P_{fc}^{high}}{P_{fc}^{max} - P_{fc}^{high}} \leq h_{fc}(i, j) \quad (36)$$

$$h_{fc}(i, j) \leq \frac{P_{fc}(i, j) - P_{fc}^{min}}{P_{fc}^{high} - P_{fc}^{min}} \quad (37)$$

Similarly, to ensure that the binary variable $i_{fc}(i, j)$ represents whether the power of FC stack j is lower than P_{fc}^{low} at time step i , the following constraints are applied,

$$\frac{P_{fc}^{low} - P_{fc}(i, j)}{P_{fc}^{low} - P_{fc}^{min}} \leq i_{fc}(i, j) \quad (38)$$

$$i_{fc}(i, j) \leq \frac{P_{fc}^{max} - P_{fc}(i, j)}{P_{fc}^{max} - P_{fc}^{low}} \quad (39)$$

By incorporating these binary control variables, the loss terms $l_{idling}(i, j)$ and $l_{high-load}(i, j)$ and Eq. (15) and Eq. (16) can be expressed as follows,

$$l_{idling}(i, j) = \frac{\Delta t \Delta V_{idling} C_{fc} (i_{fc}(i, j) + o_{fc}(i, j) - 1)}{3600 V_{drop}^{max}} \quad (40)$$

$$l_{high-load}(i, j) = \frac{\Delta t \Delta V_{high-load} C_{fc} h_{fc}(i, j)}{3600 V_{drop}^{max}} \quad (41)$$

The inclusion of the binary variable $o_{fc}(i, j)$, in the above equation ensures that the $l_{idling}(i, j)$ term is equal to zero when the FC stack j is turned off at time step i .

E. Battery Power to Current Function Reformulation

The battery power to current function, given the output power and the ECM, can be represented by the following nonlinear equation,

$$I_{bat} = \frac{V_{ocv}(SOC) - \sqrt{V_{ocv}(SOC)^2 - 4R(SOC) P_{bat}}}{2R(SOC)} \quad (42)$$

Although this function is nonlinear, a closer examination of the relationship between the output power, SOC, and battery current reveals that the surface is not excessively nonlinear, as depicted

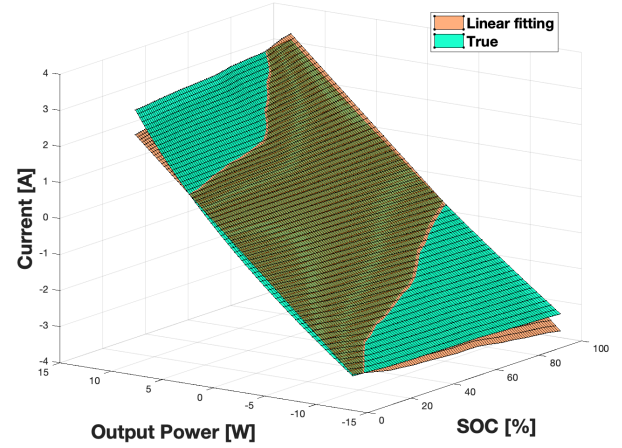


Fig. 5.

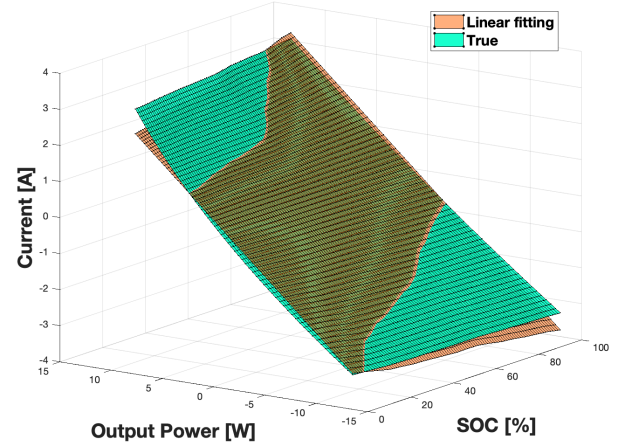


Fig. 5. The current of a 3.2 Ah battery cell across different SOC and output power ranges.

Based on this observation, a linear regression approach is employed to approximate the battery power to current relationship, $f_{bat-i}(P_{bat}(i), SOC_{bat}(i))$ described in Eq. (22). This relationship is fitted to the linear equation as,

$$I_{bat}(i) = a_{bat} P_{bat}(i) + b_{bat} SOC_{bat}(i) \quad (43)$$

where a_{bat} and b_{bat} are fitted parameters. Although the fitting result may not be perfect, the R-squared value of 0.9873 indicates a strong correlation between the fitted linear model and the actual battery dynamics. Therefore, this linear approximation sufficiently captures the general trend of the battery dynamics within the optimization framework.

It is worth noting that for a lithium iron phosphate (LFP) battery with a flat OCV-SOC curve, it is better to ignore the SOC term to achieve better approximation, particularly when the power is equal to zero. Besides, a better fitting result might be achieved using a quadratic fitting model. However, this approach would transform our MIQP problem into a Mixed Integer

Quadratically Constrained Programming (MIQCP) problem, which is more computationally intensive due to the added complexity of quadratic constraints. Despite the slight compromise in trend representation, we opted for linear approximation. This decision prioritizes real-time optimization, which is crucial in the context of our energy management system.

F. Battery Degradation Term Reformulation

According to battery degradation equation discussed in section II.B.2), in Fig. 6, the relationship between battery Ah throughput and capacity loss for different C-rates is depicted. It is observed that a lower C-rate current during charge/discharge operations leads to a higher Ah_{EOL} , indicating a longer battery life. The Ah_{EOL} values, corresponding to a 20% capacity loss, can be determined for each C-rate, representing the End-of-Life (EOL) condition of the battery.

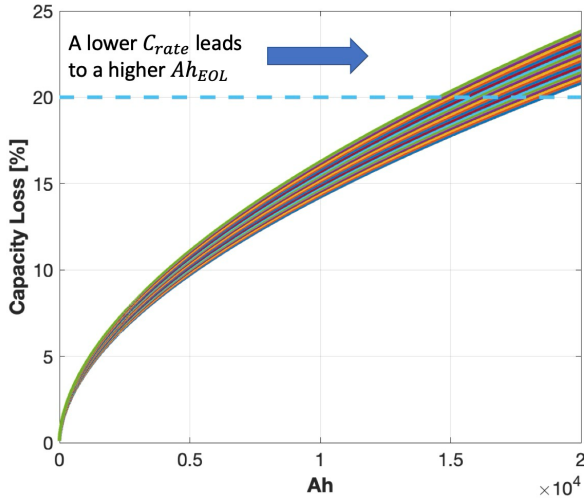


Fig. 6. Illustration of capacity loss in relation to battery Ah throughput at various C-rates.

Fig. 7 further demonstrates the relationship between the C-rate (C_{rate}) and the reciprocal of Ah_{EOL} . It is notable that this relationship exhibits a nearly linear trend. This allows for the use of linear fitting to approximate the relationship between the C-rate and $\frac{1}{Ah_{EOL}}$ as,

$$\frac{1}{Ah_{EOL}} = a_d C_{rate} + b_d \quad (44)$$

where a_d and b_d are fitting parameters obtained through linear regression.

To calculate the battery degradation loss in a sampling period, we divide the delta Ah throughput (ΔAh) in the sampling time by Ah_{EOL} , and then multiply it by the battery pack energy (E_{bat} , in kWh) and the battery price (C_{bat} , in \$/kWh). This can be expressed as,

$$l_{bat} = \frac{\Delta Ah}{2 Ah_{EOL}} Q_{bat} C_{bat} \quad (45)$$

By substituting the current value into the above equation, the function $f_{bat-loss}(I_{bat}(i))$, which represents the battery degradation loss at time step i , can be reformulated as a quadratic form with the given current,

$$I_{bat}^+(i) \geq -I_{bat}(i) \quad (46)$$

$$I_{bat}^+(i) \geq I_{bat}(i) \quad (47)$$

$$l_{bat}(i) = \left(a_d \frac{I_{bat}^+(i)^2}{Q_{bat}} + b_d I_{bat}^+(i) \right) \frac{\Delta t}{7200} Q_{bat} C_{bat} \quad (48)$$

where, $I_{bat}^+(i)$ represents the absolute value of the battery current. This formulation enables the integration of battery degradation cost into the objective function in a quadratic form.

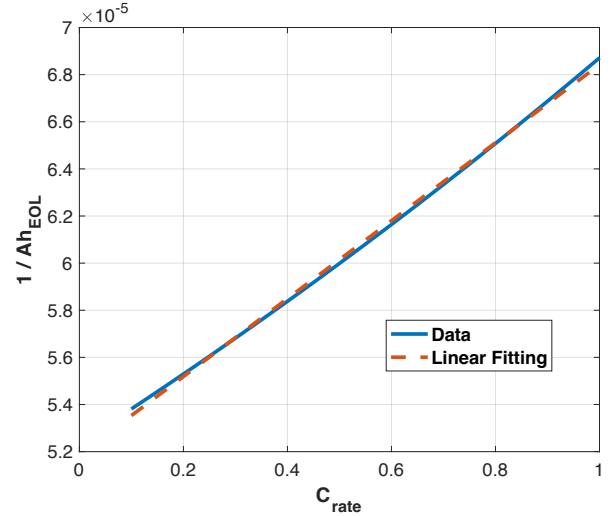


Fig. 7. C-rate vs. $\frac{1}{Ah_{EOL}}$.

G. MIQP Solver Selection

The choice of solver is critical for the online operation of the EMS because it must provide rapid and efficient optimization suitable for real-time applications.

In our study, we formulated the online EMS as a MIQP optimization problem. Given the inherent complexity introduced by integer decision variables and a quadratic objective function, we employed Gurobi [38], a well-regarded commercial software package, as our solver.

Gurobi has proven its effectiveness in solving MIQP problems by using a comprehensive branch-and-bound framework [39]. The solver first relaxes the MIQP problem by excluding the integer constraints, simplifying the problem into a Quadratic Programming (QP) task. Solving this relaxed problem is less computationally intensive and provides a lower bound for the optimal solution of the original MIQP problem. The solver then

systematically subdivides the solution space into smaller subproblems, each one individually solved or bounded. This iterative process of refining the solution and pruning the search space continues until an optimal solution is found or a predefined computational limit is reached.

IV. PERFORMANCE AND DISCUSSION

In this section, we first discuss the setup of the test environment, followed by an examination and comparison of two distinct control methods:

1. Collective Stack Control
2. Individual Stack Control

In the Collective Stack Control method, all FC stacks are treated as a single collective stack, with the same control actions applied to all stacks simultaneously. In contrast, the Individual Stack Control method controls each fuel cell stack independently, enabling tailored control actions. This approach facilitates fine-grained control of each stack to achieve optimal control goals for the whole system. Moreover, the method can account for the unique characteristics of each FC stack.

As the DP method can provide global optimization results but is limited to handling cases with few control actions, we first compare the proposed method with the DP method that employs Collective Stack Control. This comparison is aimed at demonstrating the optimality of the proposed method.

Then, we compare the Individual Stack Control and Collective Stack Control methods using the proposed method to underscore the superior performance of the Individual Stack Control method.

A. System Setup

In the simulation, the proposed method is evaluated using the Chinese Bus Driving Cycle profile, which is illustrated in Fig. 8.

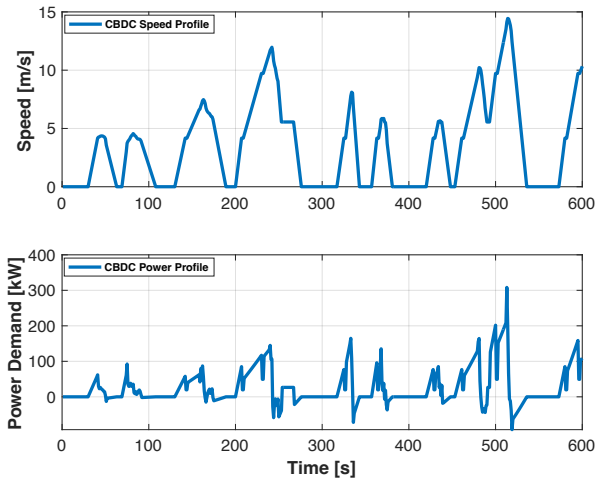


Fig. 8. CBDC speed and power profile.

For demonstration purposes, the total optimization horizon is established at 600s, with a sampling time of 1s. In the hybrid city bus under study, the powertrain includes eight FC stacks and one battery pack. Each FC stack consists of 500 individual fuel cells, each possessing an effective area of 280 cm², connected in series to deliver a maximum power output of 70 kW. The battery pack comprises 7594 individual cells, each with a capacity of 3.2 Ah, arranged in parallel to offer a total energy capacity of 90 kWh. Besides, we set the costs of the fuel cell and battery at \$960/kW [40] and \$178.41/kWh [41], respectively. We also set the initial SOC of the battery to 50%. Furthermore, to ensure the battery retains the capability to provide and absorb energy in the future, we impose a terminal constraint that limits the battery's SOC to between 47% and 53% at the end of the optimization period.

B. Benchmark approach: DP method

DP serves as a robust computational method offering globally optimal solutions to a broad range of complex optimization problems. Due to its ability to find globally optimal solutions, DP has been selected as a benchmark to evaluate the performance of the proposed algorithm in this research. However, considering the hybrid energy system in this study, which includes multiple fuel cell stacks, one noteworthy challenge arises from the high computational cost of applying DP. The computational complexity grows exponentially with the increase in the number of state variables. With multiple fuel cell stacks, treating each stack as a separate control variable would lead to a significant increase in computational complexity. Thus, for the DP application, all fuel cell stacks are considered as a single large stack, and all stacks are assigned the same control actions using the Collective Stack Control way.

In the hybrid energy system, DP involves discretizing the state and control space into finite points and solving Bellman's equation iteratively in a backward time manner [42]. This transforms the optimal control problem into a search problem within the discretized state and control space. Because the change of the FC power contribute to the FC degradation loss, besides SOC of the battery pack, the output power of the large FC stack at previous time step also is defined as the state of the system. The control is determined by the power distribution between the battery and fuel cell systems.

For each discretized state x , including battery SOC and previous FC output power, and for each time step i , the cost of all potential control actions is calculated. In this study, the grid sizes of the DP method for the SOC and FC output power are set to 0.02% and 5kW, respectively. The control, u_i , minimizing the cost is chosen. The cost not only includes the immediate cost at the current time step, but also the future cost obtained from the next time step's value function which calculated in the previous iteration as,

$$V(x_i, i) = \min_{u_i} \{C_i(x_i, u_i) + V(x_{i+1}, i + 1)\} \quad (49)$$

Following the iterative solution of Bellman's equation from the final time step to the initial time step, an optimal control policy is obtained. This policy outlines the optimal power split for each SOC at each time step. The total cost resulting from this policy can be compared to the total cost obtained from the algorithm under investigation to evaluate the proximity of the proposed algorithm to the globally optimal solution.

C. Comparative Analysis of MIQP and DP Methods with the Collective Stack Control

To evaluate the effectiveness of the proposed MIQP method, a comparative analysis is conducted with the DP approach. In this analysis, all fuel cell stacks are treated as a collective stack, and identical control actions are applied to ensure consistency (Collective Stack Control method). The objective is to examine the performance of the MIQP-based method and compare it against the global optimization achieved by DP.

Fig. 9 illustrates the power split profiles between the FC and the battery using the DP and proposed MIQP methods, respectively. The power split profiles derived from both the DP and proposed MIQP methods are remarkably similar, and the profiles nearly coincide. The battery plays a crucial role in buffering transient power spikes and providing additional power during high load conditions. This alleviates the strain on the fuel cells and reduces the occurrence of load changes and high-load conditions, which are known to contribute to fuel cell degradation. Additionally, in low load conditions, the battery effectively acts as an energy storage device, allowing the fuel cells to avoid idling and start-stop conditions by absorbing excess power through charging. Overall, the battery helps regulate and smooth out the power demand, enabling the fuel cells to operate within their optimal power range and leading to an extended lifespan for the fuel cells.

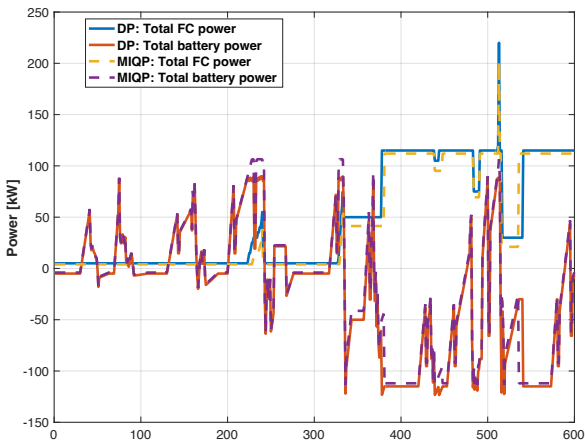


Fig. 9. Power split profiles from DP and MIQP results using the Collective Stack Control method.

It's crucial to acknowledge that the approximation of battery power to current and the reformulation of the battery degradation term serve as foundational elements for the

application of the MIQP method. Fig. 10, Fig. 11, and Fig. 12 illustrate a comparison of battery current, SOC, and degradation between the approximation and the original model, based on the optimal battery power profile obtained. This approximation accurately represents the relationship between power and current within the battery's practical operating range, thereby maintaining the accuracy of battery SOC updates. Simultaneously, the reformulation of the battery degradation term effectively encompasses the main degradation processes. Despite the fact that these simplifications result in a less complex mathematical representation of the battery's behavior, they do not compromise the validity of the results.

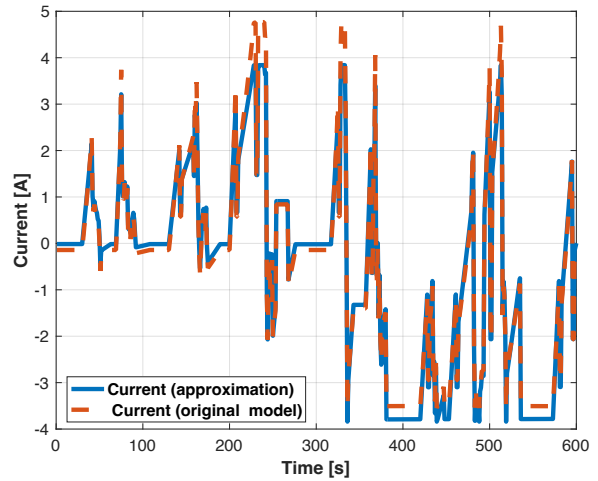


Fig. 10. Comparison of battery current: approximation vs original Model.

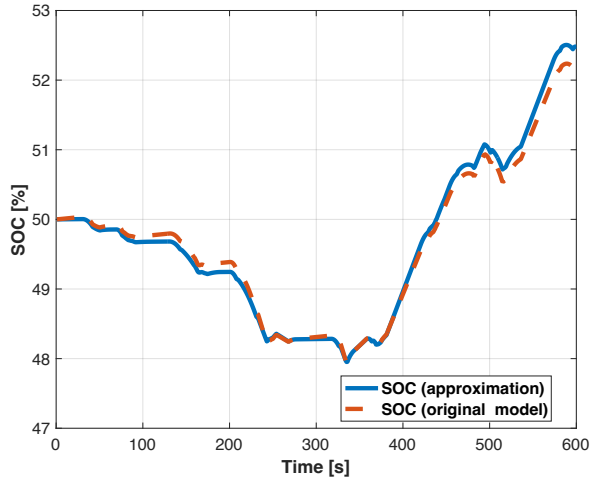


Fig. 11. Comparison of battery SOC: approximation vs original Model.

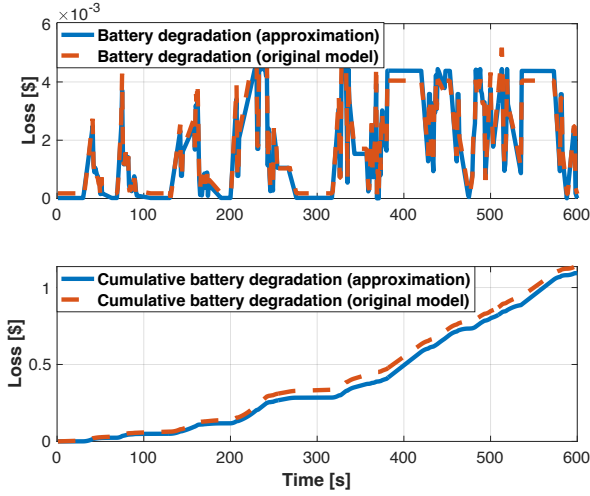


Fig. 12. Comparison of battery degradation: approximation vs original Model.

With the original power-to-current and battery degradation models in place, TABLE V displays the cumulative losses and costs of both the DP and proposed methods. The total cost is computed by combining the fuel consumption cost, FC degradation losses, and battery degradation loss. It should be noted that all costs associated with the battery are based on original models rather than approximations. Similar to the power split profiles, the cumulative loss and cost plots from both methods show significant similarities. The final total costs of the DP and proposed methods stand at \$10.24 and \$10.08, respectively. This demonstrates that the MIQP-based solution closely emulates the performance outcomes of the traditional DP approach. Remarkably, the final total cost produced by the proposed MIQP method is lower than that resulting from the DP approach.

This difference is associated with the DP method's dependency on discretizing the state and control space into finite points. While considered a global optimization method, the accuracy and optimality of the DP method can be considerably influenced by the size of the grids used in the discretization process. A fine grid size can yield near-optimal results, albeit at the cost of slower computational speed. On the other hand, a coarse grid size may lead to suboptimal outcomes. In this study, the relatively coarse grid size of the FC supply power constrains the minimal change in FC supply power, resulting in elevated FC load change loss, as shown in Fig. 13. Moreover, the coarser grid size also prevents the DP method from consistently operating within the most optimal range of the FC efficiency curve, leading to additional H₂ consumption cost, as illustrated in Fig. 14.

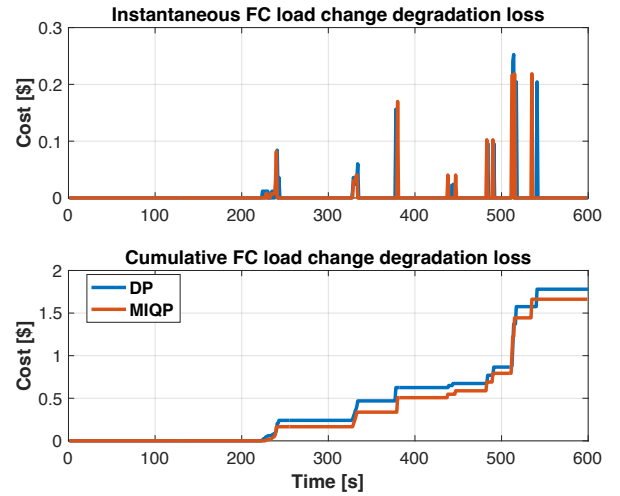


Fig. 13. The FC load change degradation losses resulting from the DP and proposed methods with Collective Stack Control.

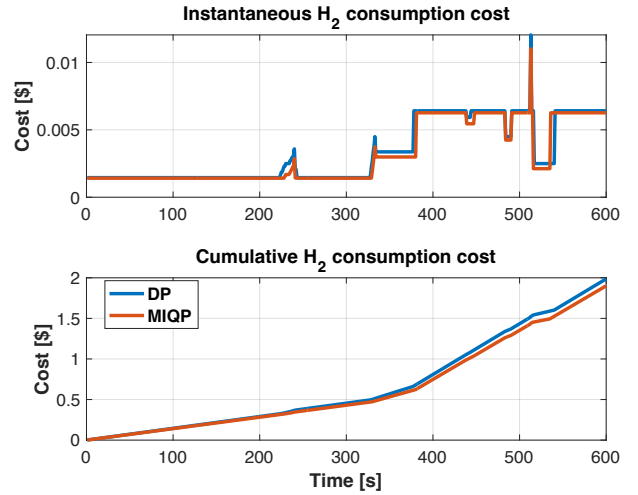


Fig. 14. The H₂ consumption cost resulting from the DP and proposed methods with Collective Stack Control.

This discretization process of the DP method introduces errors when representing continuous system dynamics and inputs. In contrast, the MIQP method utilized in the proposed approach does not rely on discretizing the state and control space. It formulates the optimization problem as a mixed-integer quadratic program, enabling it to manage continuous variables directly. This effectively eliminates the need for grid-based discretization.

Besides, the MIQP method not only ensures a comparable level of optimal results to the well-established DP method but also provides a significant reduction in computational cost. To measure the computational efficiency, we used the test computational times as a metric. The experiments were run on the same hardware and software configuration to maintain consistency. The computational times for both methods with the Collective Stack Control are presented in TABLE IV. The results clearly indicate that our proposed MIQP method

outperforms the DP method in terms of computational speed. This enhanced speed makes the MIQP method a more feasible choice for real-time applications in the energy management of hybrid systems.

TABLE IV
COMPARISON OF COMPUTATIONAL TIMES

Method	Computational Time
MIQP	14.38s
DP	32258.68s

D. MIQP with Individual Stack Control

In this subsection, we evaluate our proposed method by applying it to the individual control of eight FC stacks within the hybrid energy system, with the power demand profile presented in Section IV.A. The objective is to highlight the effectiveness and advantages of controlling each FC stack independently (Individual Stack Control), in contrast to the Collective Stack Control approach, where they are treated as a collective stack subject to the same control actions.

Using the Individual Stack Control approach and our proposed MIQP method, we allow each FC stack to have its own distinct control actions. This enables the EMS to dynamically adjust the power output of each FC stack. The power split profiles between FC stacks and the battery pack are depicted in Fig. 15. These profiles exhibit large differences when compared to the power split profiles presented in Fig. 9, illustrating the distinctions between Individual Stack Control and Collective Stack Control.

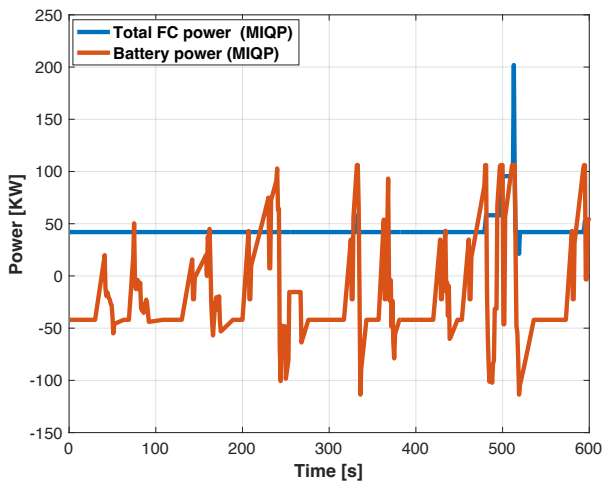


Fig. 15. Power split profiles using the proposed method and Individual Stack Control.

The role of the battery remains constant, irrespective of whether Individual Stack Control or Collective Stack Control is employed. It buffers transient power spikes, provides additional power during periods of high load, and serves as an energy

storage system when power demand is low. Thus, as illustrated in Fig. 16, the battery degradation cost exhibits no significant differences between the two control methods. In contrast, the total FC power, for the most part, remains steady or changes by only a small amount when the Individual Stack Control method is used, as demonstrated in Fig. 15. As further depicted in Fig. 17, compared to the Collective Stack Control method, the Individual Stack Control significantly reduces the FC load change degradation loss.

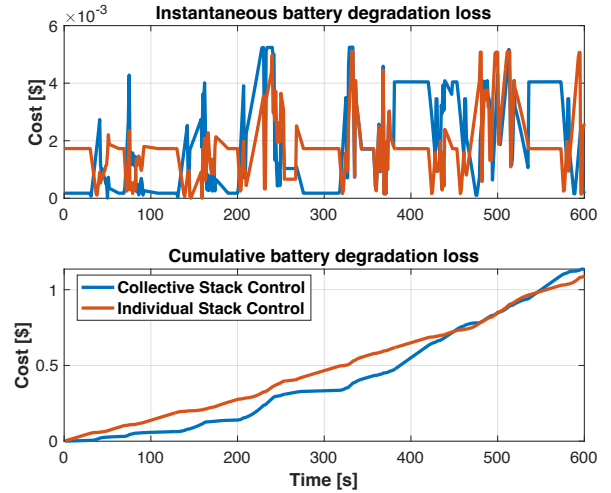


Fig. 16. Comparison of battery degradation cost between Collective Stack Control and Individual Stack Control methods.

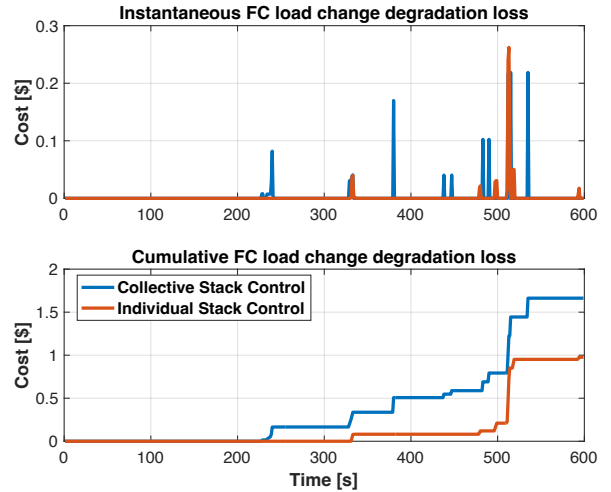


Fig. 17. Comparison of FC load change degradation costs between Collective Stack Control and Individual Stack Control methods.

The power split between each of the FC stacks is depicted in Fig. 18. Given the involvement of multiple FC stacks, a heatmap of output powers for each FC stack is introduced in Fig. 19, to more effectively illustrate the differences in supply power among the stacks. This depiction clearly shows the variability in the output power of each FC stack at the same point in time. With the flexibility to control each FC stack

individually, the proposed EMS finds the optimal combination of supply power from each FC stack. This approach ensures that the FC stacks operate within the most efficient power range, which aids in reducing fuel consumption costs. A comparison of fuel consumption costs between Individual Stack Control and Collective Stack Control using the proposed MIQP method is shown in Fig. 20. As a result, controlling each FC stack individually with the proposed EMS leads to improved operational efficiency and lower fuel consumption costs.

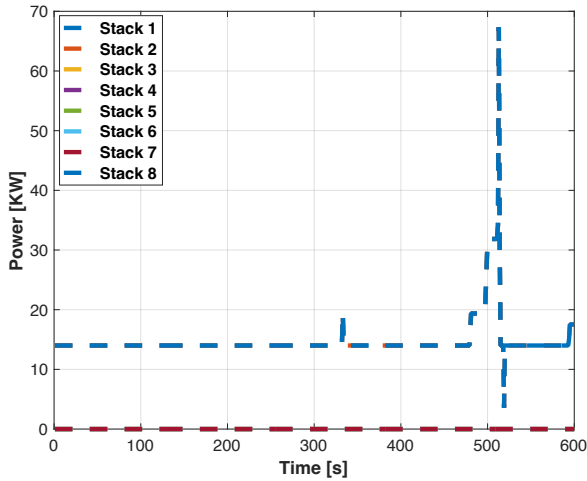


Fig. 18. Power split among different FC stacks resulting from the Individual Stack Control method.

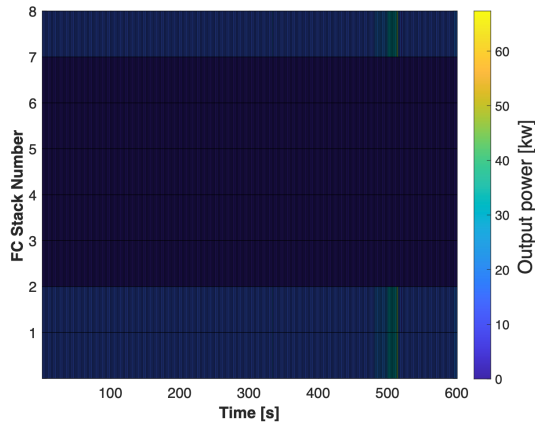


Fig. 19. Power split (heat map) among different FC stacks resulting from the Individual Stack Control method.

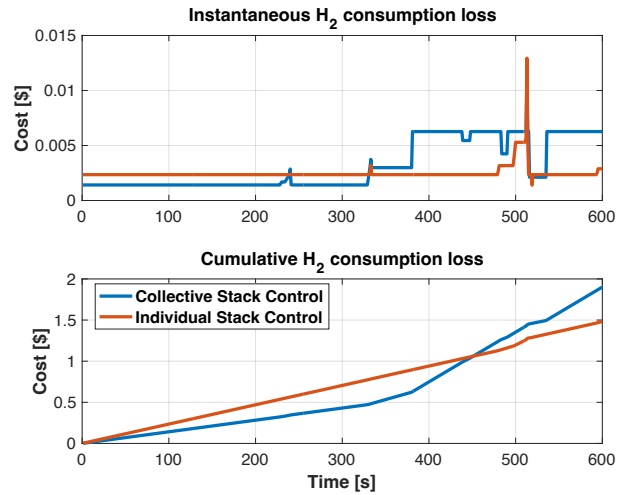


Fig. 20. Comparison of Fuel consumption costs between Collective Stack Control and Individual Stack Control methods.

In addition to maintaining each FC stack within the high-efficiency range, the Individual Stack Control method also prevents the FC stacks from remaining idle, which corresponds with the low-efficiency range. Fig. 21 presents a comparison of FC idling degradation loss between Individual Stack Control and Collective Stack Control using the proposed MIQP method. Whereas the idling degradation loss constitutes the majority of the cost under the Collective Stack Control method, the Individual Stack Control method avoids idle conditions by selectively activating the necessary number of FC stacks. The on/off conditions of each FC stack are depicted in Fig. 22. Out of eight, only three FC stacks are on, with the remaining five stacks always off. Significantly, stacks that are initially activated continue to maintain their 'on' status, whereas those that are initially 'off' persist in their 'off' state for the entire process. This method minimizes FC degradation due to on/off switching. However, since only three FC stacks are actively used, the EMS cannot perfectly handle the peak power demand at time 513s, resulting in additional FC high load degradation loss, as shown in Fig. 23.

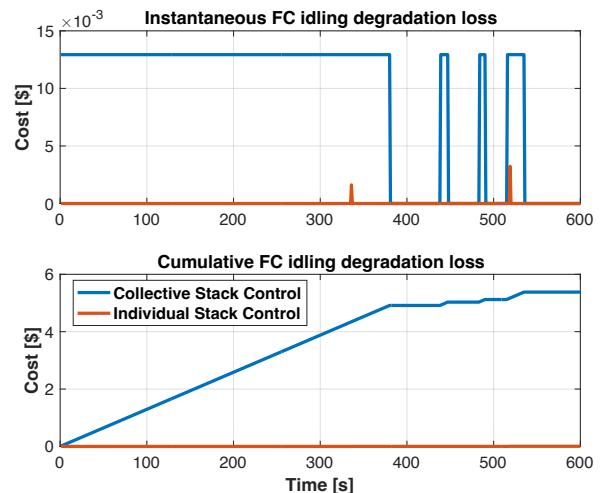


Fig. 21. Comparison of FC idling degradation costs between Collective Stack Control and Individual Stack Control methods.

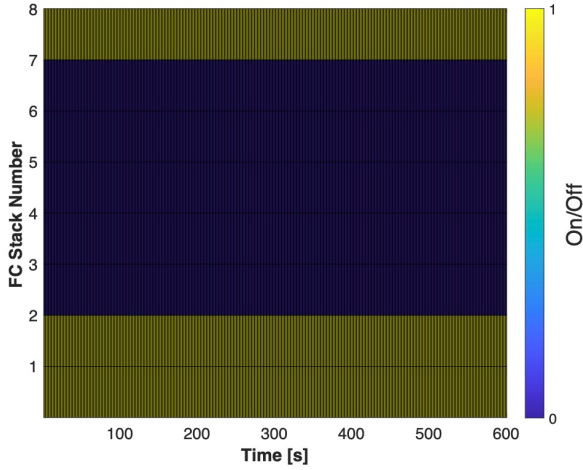


Fig. 22. On/Off status of each FC stack resulting from the Individual Stack Control method.

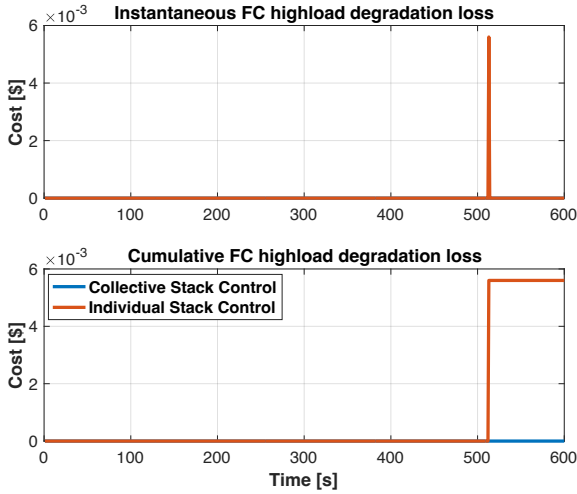


Fig. 23. Comparison of high-power load FC degradation costs between Collective Stack Control and Individual Stack Control methods.

Through comprehensive performance evaluations, the advantages of Individual Stack Control are assessed. As indicated in TABLE V, the cumulative total cost of the proposed method, which controls each FC stack individually, is \$3.56. This cost is 64.68% lower than the cost incurred when employing the Collective Stack Control method. These results underscore the benefits of improved system efficiency, enhanced load distribution, and optimal utilization of multiple FC stacks.

TABLE V
SUMMARY OF THE COSTS CROSSING DIFFERENT CONTROL METHODS

Cost (\$)	Collective Stack Control	Individual Stack Control
-----------	--------------------------	--------------------------

	DP	MIQP	MIQP
Battery degradation loss	1.1398	1.1362	1.0898
H2 consumption cost	1.9870	1.9014	1.4829
FC idling loss	5.3410	5.3798	0.0048
FC high load loss	0	0	0.0056
FC load change loss	1.7802	1.6626	0.9768
FC on/off switch loss	0	0	0
Total cost	10.24	10.08	3.5625

In addition to the benefits mentioned above, the proposed Individual Stack Control method also enables configuration of different FC stacks with their specific parameters. This capability could significantly enhance the performance of the EMS when different types of FC stacks are deployed in the system. Furthermore, the Individual Stack Control approach offers flexibility in system operation and maintenance. It supports targeted monitoring and maintenance of specific stacks, simplifying troubleshooting and stack replacement tasks. This individualized control of FC stacks also strengthens fault tolerance and system resilience. For example, the failure of a single stack would not have a significant impact on the overall system performance [16].

V. CONCLUSION

This study introduces an innovative MIQP-based EMS for an FC and battery hybrid system with multiple FC stacks. The analysis and evaluation of the proposed method yield valuable insights into the advantages and practicality of managing each FC stack independently, an approach referred to as Individual Stack Control, in hybrid energy systems.

Comparing the proposed method to DP under Collective Stack Control—which treats all FC stacks as a unified entity under the same control actions—illustrates that the MIQP method can match the DP approach's performance. Remarkably, the MIQP method achieves this with significantly reduced computational time, being 2243 times faster than the DP method. This finding suggests that the MIQP method offers high efficiency both in terms of comparable results and significantly reduced computational resource requirements—an advantage in real-time or online systems.

Furthermore, the study reveals that adopting Individual Stack Control, which manages each FC stack independently, can substantially enhance the performance of the EMS. This method leads to significant reductions in fuel consumption and costs related to FC and battery degradation, resulting in an

impressive cost reduction of 64.68% in the scenario examined in this study.

The newly proposed MIQP-based EMS lays a robust foundation for future exploration and development in the optimization and control of multi-stack systems. While this study has centered on the application of this method to city buses, the technique could be readily adapted to similar systems, such as trucks and ocean-going vessels, by adjusting the system configuration parameters.

VI. REFERENCES

- [1] T. Zhang, P. Wang, H. Chen, and P. Pei, "A review of automotive proton exchange membrane fuel cell degradation under start-stop operating condition," *Applied Energy*, vol. 223, pp. 249–262, Aug. 2018, doi: 10.1016/j.apenergy.2018.04.049.
- [2] B. Widera, "Renewable hydrogen implementations for combined energy storage, transportation and stationary applications," *Thermal Science and Engineering Progress*, vol. 16, p. 100460, May 2020, doi: 10.1016/j.tsep.2019.100460.
- [3] L. Vichard, N. Y. Steiner, N. Zerhouni, and D. Hissel, "Hybrid fuel cell system degradation modeling methods: A comprehensive review," *Journal of Power Sources*, vol. 506, p. 230071, Sep. 2021, doi: 10.1016/j.jpowsour.2021.230071.
- [4] P. Ren, P. Pei, Y. Li, Z. Wu, D. Chen, and S. Huang, "Degradation mechanisms of proton exchange membrane fuel cell under typical automotive operating conditions," *Progress in Energy and Combustion Science*, vol. 80, p. 100859, Sep. 2020, doi: 10.1016/j.pecs.2020.100859.
- [5] N. Marx, L. Boulon, F. Gustin, D. Hissel, and K. Agbossou, "A review of multi-stack and modular fuel cell systems: Interests, application areas and on-going research activities," *International Journal of Hydrogen Energy*, vol. 39, no. 23, pp. 12101–12111, Aug. 2014, doi: 10.1016/j.ijhydene.2014.05.187.
- [6] Y. Wang, S. J. Moura, S. G. Advani, and A. K. Prasad, "Power management system for a fuel cell/battery hybrid vehicle incorporating fuel cell and battery degradation," *International Journal of Hydrogen Energy*, vol. 44, no. 16, pp. 8479–8492, Mar. 2019, doi: 10.1016/j.ijhydene.2019.02.003.
- [7] J. Bernard, S. Delprat, T. M. Guerra, and F. N. Büchi, "Fuel efficient power management strategy for fuel cell hybrid powertrains," *Control Engineering Practice*, vol. 18, no. 4, pp. 408–417, Apr. 2010, doi: 10.1016/j.conengprac.2009.12.009.
- [8] K. Ettihir, L. Boulon, and K. Agbossou, "Optimization-based energy management strategy for a fuel cell/battery hybrid power system," *Applied Energy*, vol. 163, pp. 142–153, Feb. 2016, doi: 10.1016/j.apenergy.2015.10.176.
- [9] H. Peng *et al.*, "A scalable, causal, adaptive rule-based energy management for fuel cell hybrid railway vehicles learned from results of dynamic programming," *eTransportation*, vol. 4, p. 100057, May 2020, doi: 10.1016/j.etrans.2020.100057.
- [10] H.-B. Yuan, W.-J. Zou, S. Jung, and Y.-B. Kim, "Optimized rule-based energy management for a polymer electrolyte membrane fuel cell/battery hybrid power system using a genetic algorithm," *International Journal of Hydrogen Energy*, vol. 47, no. 12, pp. 7932–7948, Feb. 2022, doi: 10.1016/j.ijhydene.2021.12.121.
- [11] P. M. Muñoz, G. Correa, M. E. Gaudiano, and D. Fernández, "Energy management control design for fuel cell hybrid electric vehicles using neural networks," *International Journal of Hydrogen Energy*, vol. 42, no. 48, pp. 28932–28944, Nov. 2017, doi: 10.1016/j.ijhydene.2017.09.169.
- [12] B. Xu, J. Shi, S. Li, H. Li, and Z. Wang, "Energy consumption and battery aging minimization using a Q-learning strategy for a battery/ultracapacitor electric vehicle," *Energy*, vol. 229, p. 120705, Aug. 2021, doi: 10.1016/j.energy.2021.120705.
- [13] X. Tang, H. Zhou, F. Wang, W. Wang, and X. Lin, "Longevity-conscious energy management strategy of fuel cell hybrid electric Vehicle Based on deep reinforcement learning," *Energy*, vol. 238, p. 121593, Jan. 2022, doi: 10.1016/j.energy.2021.121593.
- [14] "Power sharing for efficiency optimisation into a multi fuel cell system." <https://ieeexplore.ieee.org/abstract/document/6864614/> (accessed Jun. 05, 2023).
- [15] A. Macias Fernandez, M. Kandidayeni, L. Boulon, and H. Chaoui, "An Adaptive State Machine Based Energy Management Strategy for a Multi-Stack Fuel Cell Hybrid Electric Vehicle," *IEEE Transactions on Vehicular Technology*, vol. 69, no. 1, pp. 220–234, Jan. 2020, doi: 10.1109/TVT.2019.2950558.
- [16] "Online energy management strategy considering fuel cell fault for multi-stack fuel cell hybrid vehicle based on multi-agent reinforcement learning," *Applied Energy*, vol. 328, p. 120234, Dec. 2022, doi: 10.1016/j.apenergy.2022.120234.
- [17] J. Hou and Z. Song, "A hierarchical energy management strategy for hybrid energy storage via vehicle-to-cloud connectivity," *Applied Energy*, vol. 257, p. 113900, Jan. 2020, doi: 10.1016/j.apenergy.2019.113900.
- [18] J. Shi, B. Xu, Y. Shen, and J. Wu, "Energy management strategy for battery/supercapacitor hybrid electric city bus based on driving pattern recognition," *Energy*, p. 122752, Nov. 2021, doi: 10.1016/j.energy.2021.122752.
- [19] Z. Song, H. Hofmann, J. Li, J. Hou, X. Han, and M. Ouyang, "Energy management strategies comparison for electric vehicles with hybrid energy storage system," *Applied Energy*, vol. 134, pp. 321–331, Dec. 2014, doi: 10.1016/j.apenergy.2014.08.035.
- [20] J. Wang *et al.*, "Cycle-life model for graphite-LiFePO4 cells," *Journal of Power Sources*, vol. 196, no. 8, pp. 3942–3948, Apr. 2011, doi: 10.1016/j.jpowsour.2010.11.134.

- [21] H. E. Perez, X. Hu, S. Dey, and S. J. Moura, "Optimal Charging of Li-Ion Batteries With Coupled Electro-Thermal-Aging Dynamics," *IEEE Transactions on Vehicular Technology*, vol. 66, no. 9, pp. 7761–7770, Sep. 2017, doi: 10.1109/TVT.2017.2676044.
- [22] S. J. Peighambari, S. Rowshanzamir, and M. Amjadi, "Review of the proton exchange membranes for fuel cell applications," *International Journal of Hydrogen Energy*, vol. 35, no. 17, pp. 9349–9384, Sep. 2010, doi: 10.1016/j.ijhydene.2010.05.017.
- [23] F. Odeim, J. Roes, L. Wülbeck, and A. Heinzl, "Power management optimization of fuel cell/battery hybrid vehicles with experimental validation," *Journal of Power Sources*, vol. 252, pp. 333–343, Apr. 2014, doi: 10.1016/j.jpowsour.2013.12.012.
- [24] O. Z. Sharaf and M. F. Orhan, "An overview of fuel cell technology: Fundamentals and applications," *Renewable and Sustainable Energy Reviews*, vol. 32, pp. 810–853, Apr. 2014, doi: 10.1016/j.rser.2014.01.012.
- [25] P. Pei, Q. Chang, and T. Tang, "A quick evaluating method for automotive fuel cell lifetime," *International Journal of Hydrogen Energy*, vol. 33, no. 14, pp. 3829–3836, Jul. 2008, doi: 10.1016/j.ijhydene.2008.04.048.
- [26] Y. Zhou, A. Ravey, and M.-C. Péra, "Real-time cost-minimization power-allocating strategy via model predictive control for fuel cell hybrid electric vehicles," *Energy Conversion and Management*, vol. 229, p. 113721, Feb. 2021, doi: 10.1016/j.enconman.2020.113721.
- [27] M. Jouin, R. Gouriveau, D. Hissel, M.-C. Péra, and N. Zerhouni, "Degradations analysis and aging modeling for health assessment and prognostics of PEMFC," *Reliability Engineering & System Safety*, vol. 148, pp. 78–95, Apr. 2016, doi: 10.1016/j.ress.2015.12.003.
- [28] G. Wang, F. Huang, Y. Yu, S. Wen, and Z. Tu, "Degradation behavior of a proton exchange membrane fuel cell stack under dynamic cycles between idling and rated condition," *International Journal of Hydrogen Energy*, vol. 43, no. 9, pp. 4471–4481, Mar. 2018, doi: 10.1016/j.ijhydene.2018.01.020.
- [29] G. J. M. Janssen, E. F. Sitters, and A. Pfrang, "Proton-exchange-membrane fuel cells durability evaluated by load-on/off cycling," *Journal of Power Sources*, vol. 191, no. 2, pp. 501–509, Jun. 2009, doi: 10.1016/j.jpowsour.2009.02.027.
- [30] R. Petrone, D. Hissel, M. C. Péra, D. Chamagne, and R. Gouriveau, "Accelerated stress test procedures for PEM fuel cells under actual load constraints: State-of-art and proposals," *International Journal of Hydrogen Energy*, vol. 40, no. 36, pp. 12489–12505, Sep. 2015, doi: 10.1016/j.ijhydene.2015.07.026.
- [31] K. Song, H. Chen, P. Wen, T. Zhang, B. Zhang, and T. Zhang, "A comprehensive evaluation framework to evaluate energy management strategies of fuel cell electric vehicles," *Electrochimica Acta*, vol. 292, pp. 960–973, Dec. 2018, doi: 10.1016/j.electacta.2018.09.166.
- [32] D. Zhou, Y. Wu, F. Gao, E. Breaz, A. Ravey, and A. Miraoui, "Degradation Prediction of PEM Fuel Cell Stack Based on Multiphysical Aging Model With Particle Filter Approach," *IEEE Transactions on Industry Applications*, vol. 53, no. 4, pp. 4041–4052, Jul. 2017, doi: 10.1109/TIA.2017.2680406.
- [33] R. Borup *et al.*, "Scientific Aspects of Polymer Electrolyte Fuel Cell Durability and Degradation," *Chem. Rev.*, vol. 107, no. 10, pp. 3904–3951, Oct. 2007, doi: 10.1021/cr050182l.
- [34] J. Zhao, Z. Tu, and S. H. Chan, "Carbon corrosion mechanism and mitigation strategies in a proton exchange membrane fuel cell (PEMFC): A review," *Journal of Power Sources*, vol. 488, p. 229434, Mar. 2021, doi: 10.1016/j.jpowsour.2020.229434.
- [35] H. Li *et al.*, "PEM Fuel Cell Contamination: Effects of Operating Conditions on Toluene-Induced Cathode Degradation," *J. Electrochem. Soc.*, vol. 156, no. 2, p. B252, Dec. 2008, doi: 10.1149/1.3040212.
- [36] M. W. Fowler, R. F. Mann, J. C. Amphlett, B. A. Peppley, and P. R. Roberge, "Incorporation of voltage degradation into a generalised steady state electrochemical model for a PEM fuel cell," *Journal of Power Sources*, vol. 106, no. 1, pp. 274–283, Apr. 2002, doi: 10.1016/S0378-7753(01)01029-1.
- [37] H. Chen, P. Pei, and M. Song, "Lifetime prediction and the economic lifetime of Proton Exchange Membrane fuel cells," *Applied Energy*, vol. 142, pp. 154–163, Mar. 2015, doi: 10.1016/j.apenergy.2014.12.062.
- [38] "Gurobi Optimizer Reference Manual," *Gurobi Optimization*. <https://www.gurobi.com/documentation/current/refman/index.html> (accessed Jul. 13, 2023).
- [39] "Mixed-Integer Programming (MIP) – A Primer on the Basics," *Gurobi Optimization*. <https://www.gurobi.com/resources/mixed-integer-programming-mip-a-primer-on-the-basics/> (accessed Jul. 13, 2023).
- [40] S. Di Micco, L. Mastropasqua, V. Cigolotti, M. Minutillo, and J. Brouwer, "A framework for the replacement analysis of a hydrogen-based polymer electrolyte membrane fuel cell technology on board ships: A step towards decarbonization in the maritime sector," *Energy Conversion and Management*, vol. 267, p. 115893, Sep. 2022, doi: 10.1016/j.enconman.2022.115893.
- [41] K. Li, J. Zhou, C. Jia, F. Yi, and C. Zhang, "Energy sources durability energy management for fuel cell hybrid electric bus based on deep reinforcement learning considering future terrain information," *International Journal of Hydrogen Energy*, Jun. 2023, doi: 10.1016/j.ijhydene.2023.05.311.
- [42] J. Shi, B. Xu, X. Zhou, and J. Hou, "A cloud-based energy management strategy for hybrid electric city bus considering real-time passenger load prediction," *Journal of Energy Storage*, vol. 45, p. 103749, Jan. 2022, doi: 10.1016/j.est.2021.103749.

